Acta Crystallographica Section D
Biological Crystallography
ISSN 0907-4449

Serendipitous SAD phasing of an echinomycin–$(ACGTACGT)_2$ bisintercalation complex

Jose A. Cuesta-Seijo,[a] Manfred S. Weiss[b] and George M. Sheldrick[a]*

[a]Department of Structural Chemistry, University of Göttingen, Tammannstrasse 4, D37077 Göttingen, Germany, and [b]EMBL Hamburg Outstation, c/o DESY, Notkestrasse 85, D-22603 Hamburg, Germany

Correspondence e-mail: gsheldr@shelx.uni-ac.gwdg.de

Received 7 November 2005
Accepted 31 January 2006

PDB Reference: echinomycin–$(ACGTACGT)_2$ complex, 2adw, r2adwsf.

A new crystal form was obtained for the complex between $(ACGTACGT)_2$ and echinomycin and X-ray data were collected to 1.6 Å. The structure was phased by the SAD method based on a single unexpected anomalous scatterer that could be identified as a mixture of nickel and zinc by measurements of the anomalous scattering at different wavelengths. This cation is coordinated by two guanines from two different duplexes and four water molecules. The structure resembles previously reported crystal structures of DNA–echinomycin complexes, except that three of the eight base pairs flanking the echinomycin bisintercalator sites have the Watson–Crick rather than the Hoogsteen configuration. Hoogsteen binding was found for the corresponding base pairs of the crystallographically independent duplex, indicating that the two configurations are very close in energy.

1. Introduction

Echinomycin, a depsipeptide antibiotic from *Streptomyces*, is the canonical representative of the quinoxaline antibiotics. The molecules of this family bind to duplex DNA by bisintercalation both *in vitro* (Waring & Wakelin, 1974; Wakelin & Waring, 1976; Waring, 1981, 1993) and *in vivo* (May *et al.*, 2004), interfering with both replication and transcription (Ward *et al.*, 1965; Sato *et al.*, 1967). These antibiotics are undergoing clinical trials as anticancer agents (Park *et al.*, 2004). The interactions of echinomycin with DNA have been studied extensively by biochemical (Quigley *et al.*, 1986; Gallego, Luque, Orozco & Gago, 1994; Gallego, Luque, Orozco, Burgos *et al.*, 1994) and biological methods (Leslie & Fox, 2002; May *et al.*, 2004). Bisintercalation is found to occur preferentially but not exclusively (Tseng *et al.*, 2005) around CG steps of the DNA (Sayers & Waring, 1993). All previous crystallographic studies of complexes of echinomycin (Ughetto *et al.*, 1985; Cuesta-Seijo & Sheldrick, 2005) and the closely related triostin A (Wang *et al.*, 1984, 1986; Quigley *et al.*, 1986) with duplex DNA have found the base pairs within the bisintercalation site to adopt the Watson–Crick base-pairing mode, while in all cases base pairs flanking these sites exhibited Hoogsteen pairing. In Hoogsteen base pairs, hydrogen bonds are formed between N7 and N6 of the adenines and N3 and O4 of the thymines or between N7 and O6 of the guanines and N3 and N4 of the cytosines, with the purines rotated around the glycosidic bond to adopt the *syn* conformation. In contrast, footprinting studies (Jeppesen & Nielsen, 1988; Portugal *et al.*, 1988; McLean *et al.*, 1989; Sayers & Waring, 1993) found no evidence of Hoogsteen base pairs, while NMR studies (Gao & Patel, 1988; Gilbert & Feigon, 1991, 1992) found a mixture of Hoogsteen and Watson–Crick pairing except for the complexes of echinomycin with

Table 1
Data and refinement statistics.

Values for the highest resolution shells (or standard uncertainties in the case of the unit-cell parameters) are given in parentheses.

Sequence	$(ACGTACGT)_2$
Space group	$P4_22_12$
Unit-cell parameters	
$a = b$ (Å)	80.904 (16)
c (Å)	48.194 (10)
Wavelength (Å)	0.9000
Resolution (Å)	1.60 (1.70–1.60)
Total reflections	269046
Unique reflections	21134
Completeness (%)	97.6 (96.3)
R_{int} (%)	7.16 (39.41)
$I/\sigma(I)$	18.70 (5.33)
No. of data/restraints/parameters	19031/15202/10153
R (%)	17.96
R_{free} (%)	22.15
PDB code	2adw

$(ACGT)_2$ and with $(ACGTACGT)_2$ at 274 K, which were found to contain only Hoogsteen base pairs flanking the bisintercalation sites.

2. Materials and methods

2.1. Crystallization and data collection

Echinomycin was purchased from Sigma–Aldrich (E-4392) and used without further purification. The oligonucleotide with sequence ACGTACGT was purchased already purified by HPLC from Carl Roth GmbH and was used without further purification. Echinomycin is not water-soluble and so was dissolved in methanol; the oligonucleotide was dissolved in water. The solutions were mixed to give a stock solution containing 50% water and 50% methanol with a DNA concentration of 0.5 mg ml^{-1} and an echinomycin:DNA molar ratio of 1.1:1.0 (considering the DNA as a single chain). Mole ratios of less than 1:1 would produce a mixture of uncomplexed DNA duplexes and duplexes bound to two antibiotic molecules.

The best crystal was obtained using the hanging-drop method from a drop containing 25 µl stock solution and 1 µl reservoir solution containing 32% PEG 200, 6% PEG 3350, 0.1 *M* MES buffer pH 6.0 and 0.02 *M* spermine tetrachloride. The hanging drop was incubated over 1 ml reservoir solution at 293 K. A needle-shaped crystal 1.25 mm long and 0.05 mm in diameter grew over more than one month. The crystal was mounted in a nylon loop and frozen by plunging it into liquid nitrogen without the need for cryoprotectant. Data collection was carried out at 100 K on beamline 14.1 at BESSY, Berlin at a wavelength of 0.900 Å. The data were integrated and scaled with *XDS* (Kabsch, 1993) to a resolution of 1.6 Å. The crystals were tetragonal, with space group $P4_22_12$ and unit-cell parameters $a = b = 80.904$ (16), $c = 48.194$ (10) Å.

The main difference in crystallization conditions from those reported for a hexagonal complex of echinomycin with the same oligonucleotide (Cuesta-Seijo & Sheldrick, 2005) was the absence of $MgCl_2$ from the crystallization cocktail. Crystals of the hexagonal form were grown in the presence of Mg^{2+} ions, but they also grew in the absence of magnesium and often grew in the same drops as the tetragonal crystals. The tetragonal crystal form could never be obtained from drops containing added $MgCl_2$, but we cannot rule out the possibility that low Mg^{2+} concentrations were present in the DNA.

2.2. Structure solution and refinement

The structure was solved by the SAD (single-wavelength anomalous diffraction) method with the help of the *hkl2map* GUI (Pape & Schneider, 2004). Although no heavier atoms than chlorine were knowingly included in the crystallization cocktail, anomalous differences calculated with *XPREP* (Bruker AXS) showed a significant anomalous signal extending to approximately 2.5 Å. This was used to locate the anomalous scatterer(s) with *SHELXD* (Sheldrick *et al.*, 2001; Schneider & Sheldrick, 2002). The best solution had a CC(all) of 33.9% and CC(weak) of 19.5%, with only one significant site in the asymmetric unit. 500 cycles of density modification with *SHELXE* (Sheldrick, 2002) with a solvent content of 45% yielded an interpretable electron-density map (contrast 0.70, connectivity 0.94, pseudo-free correlation coefficient 86.7%) in which an initial model could be traced by hand. The FOM-weighted mean phase error relative to the final refined model was 37.9° and the map correlation coefficient was 0.88 (a more recent version of *SHELXE* improved these to 30.6° and 0.92, respectively).

Restrained anisotropic refinement with riding H atoms was carried out with *SHELXL* (Sheldrick & Schneider, 1997). The diffraction pattern was anisotropic and the adoption of an anisotropic model for refinement at 1.6 Å was accompanied by a decrease of 3.1% in the free R factor (Brünger, 1992). The data-processing and refinement statistics are given in Table 1.

3. Results and discussion

3.1. The origin of the anomalous scattering

The anomalous scattering was found to originate from a single site occupied by an octahedrally coordinated metal with four water molecules and N7 of two guanines as ligands. The cation was presumably an impurity in the drops and refinement with any first-row transition metal gave good model geometry and statistics. Anomalous scattering methods were used to elucidate the nature of this atom.

The original crystal was no longer available, so a second crystal was used to obtain fluorescence scans. This crystal was grown by the hanging-drop method at 293 K from the same stock solution as before with a reservoir composed of 30% PEG 200, 0.1 *M* MES buffer pH 6 and 0.02 *M* spermine tetrachloride. The drop was composed of 20 µl stock solution and 1 µl reservoir solution. A 0.6 mm long and 0.15 mm thick crystal was used for the measurements without the need for cryoprotectant. Five fluorescence scans were collected on the EMBL X31 beamline at the DORIS storage ring, DESY, Hamburg. The sampled energies ranged from 9559 to 9759 eV for the zinc absorption edge, from 8879 to 9079 eV for copper,

Table 2
The expected values of f'' for potential atoms (in electrons) based upon the theoretical approximation developed by Cromer & Liberman (1970).

These values were retrieved from the internet site of the Biomolecular Structure Center at the University of Washington, Seattle, USA (http://www.bmsc.washington.edu/scatter/AS_periodic.html).

λ (Å)	f'' (Zn)	f'' (Cu)	f'' (Ni)	f'' (Co)	f'' (P)	f'' (Mg)	f'' (Na)
1.000	2.55	2.29	2.02	1.78	0.19	0.07	0.05
1.362	0.54	3.80	3.37	2.98	0.34	0.14	0.10
1.470	0.62	0.54	3.82	3.33	0.40	0.16	0.11
1.520	0.66	0.58	0.50	3.53	0.42	0.17	0.12

from 8232 to 8432 eV for nickel, from 7609 to 7809 eV for cobalt and from 7012 to 7220 eV for iron. The beamline construction did not allow us to reach the manganese absorption edge and the limitations of the hardware and weak beam resulted in very noisy scans. Absorption edges and an increase in the baseline level between the low- and high-energy side of the peak could only be identified for zinc and nickel.

Four data sets were also measured from a third crystal in order to obtain anomalous maps to unambiguously identify the anomalous scatterers in the crystal. This crystal was grown in the same way as the second crystal except that the temperature was 283 K and 5% PEG 3350 was added to the reservoir solution. This drop rendered a needle-shaped crystal that was mounted in a nylon loop without the need for cryoprotectant. Four data sets were obtained with a total oscillation angle of 180° and 1° per image, with the experimental parameters adjusted in each data set to obtain similar counting statistics for the strong reflections. The four wavelengths chosen, 1.000, 1.362, 1.470 and 1.520 Å, include the low- and high-energy sides of the absorption edges of zinc, copper and nickel (Table 2).

The four data sets from the third crystal were collected without changing the position of the crystal, which was almost fully bathed in the beam. They extended to 2.8 Å in the best case (1.00 Å wavelength) and to 3.0 Å in the worst. Since the diffraction patterns were rather anisotropic and only the anomalous signal was required for this experiment, a common resolution cutoff of 4 Å was applied to all of them for integration with *DENZO* (Otwinowski & Minor, 1997); all four data sets were scaled with *SADABS* (Bruker AXS). Owing to the low flux of beamline X31, the modest diffracting power of the crystal, the anisotropic diffraction and the presence of satellites, the four data sets had relatively high values of $R_{\rm int}$: 8.5% at a wavelength of 1.00 Å, 9.7% at 1.36 Å, 10.0% at 1.47 Å and 9.9% at 1.52 Å.

Table 3
Statistics for the anomalous electron-density maps.

Wavelength (Å)	1.000	1.362	1.470	1.520
Electron density at metal site (σ units)	10.8	4.9	6.1	1.03
Electron density at nearest peak (σ units)	10.9	5.1	6.8	—
Distance of this peak from metal site (Å)	0.13	0.48	0.77	—
Highest other peak in the map (σ units)	3.9	4.2	4.9	4.5

Refinement was carried out against the 1.6 Å native data with an Ni atom provisionally assigned to the metal site and the anomalous differences at each wavelength and an almost fully refined model were used to calculate phases for the anomalous Fourier maps using *SHELXE* (Sheldrick, 2002). In the meantime, the version of *SHELXE* used for this work has become the standard release and instructions for calculating these anomalous Fouriers are provided in the documentation. Five cycles of density modification starting with phases from this model were employed for each data set with an estimated solvent fraction of 0.4; an artificial B factor of 30 Å^2 was applied to the coefficients for the anomalous map to minimize noise. The results are presented in Table 3. We performed similar calculations using the programs available in the *CCP*4 system, but the resulting maps were appreciably more noisy; the weighting scheme used in *SHELXE* may be more appropriate.

The level of the anomalous electron density at the metal site increases on moving from the low- to the high-energy sides of the absorption edges of nickel and zinc, but not for copper. The distances of the highest peak from the metal site are acceptable in view of the effective resolution (about 3 Å) and the high noise level of the maps. At lower energies (but still above the absorption edges of elements lighter than nickel) the anomalous electron density is very low. This is in agreement with the information from the fluorescence scans and suggests a metal site occupied exclusively by a combination of nickel and zinc. Although the signal for zinc seems to be stronger than that for nickel, we considered the data to be too noisy to allow quantitative interpretation. A metal site occupied by nickel and zinc, both with occupancies of 50%, was adopted for the final rounds of structure refinement.

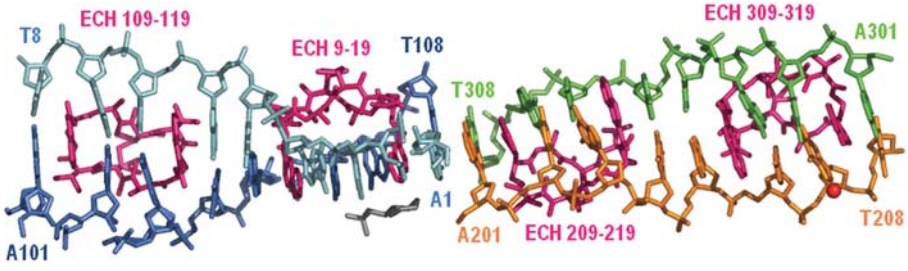

Figure 1
The asymmetric unit of the structure. Water molecules have been omitted for clarity. The four independent DNA chains are shown in cyan, blue, green and orange and the echinomycins are shown in pink; the red sphere is the metal site and the MES molecule is represented in grey.

3.2. Overall description of the crystal structure

The asymmetric unit contains four independent DNA chains forming two antiparallel duplexes, with four echinomycin molecules bisintercalating around all four CG steps in the minor groove. The DNA bases are numbered A1–T8 and A101–T108 for the first

duplex and A201–T208 and A301–T308 for the second duplex, with the echinomycin chromophores numbered 9 and 19 exhibiting bisintercalation around C2 and G3, chromophores 109 and 119 around C102 and G103 *etc*., as shown in Fig. 1. The metal cation forms an octahedral complex with four water molecules and N7 of both G7 and G207, with the N atoms occupying axial coordination positions. A molecule of the buffer MES (2-morpholinoethanesulfonic acid) and 86 waters are present in the asymmetric unit in the final model. The crystal thus contains two fully independent copies of the biologically relevant unit: a DNA duplex with two echinomycins in the minor groove.

The two DNA duplexes in the asymmetric unit form a stack with A201 lying over A1 and T308 over T8, with inversion of the helix direction. The base pair formed by T208 and A301 stacks onto its symmetry equivalent in a similar way, thymine lying over thymine and adenine over adenine, again with inversion of the chain direction at this point. The base pair T8–A101 does not stack onto other nucleobases and so the crystal lacks the infinite columns of stacked base pairs observed in other crystal structures of DNA complexes with quinoxaline antibiotics. The metal cation mediates a contact between G7 and G207 (Fig. 2) connecting the two duplexes, which are also linked by lateral hydrogen-bond contacts between the base pairs T208–A301 and T8–A101. Two independent continuous solvent channels run parallel to the *c* axis of the crystal, the larger of them having a cross-section of 55 × 35 Å.

3.3. Echinomycin structure and binding

As observed in Cuesta-Seijo & Sheldrick (2005), echinomycin acts as a rigid body with a well defined structure almost unperturbed by the DNA environment. All four independent echinomycin molecules in this structure were superimposed on that of PDB entry 1xvn (76 atoms superimposed, ignoring minor disordered conformations); the resulting root-mean-square deviations (r.m.s.d.s) are 0.34 Å for echinomycin 9–19, 0.53 Å for 109–119, 0.21 Å for 209–219 and 0.16 Å for 309–319 (Fig. 3). The r.m.s.d.s are a little higher for the first two echinomycins, those with at least one Watson–Crick base pair outside the bisintercalation side, but the differences are very small and are concentrated in the flexible ester bonds and valine side chains which are not directly involved in DNA binding.

Only echinomycin 209–219 is found in a single orientation in the crystal. The other three can bind in two different orientations related by a twofold rotation around the centre of the depsipeptide ring, as observed by Cuesta-Seijo & Sheldrick (2005). The same procedure for modelling the disorder was also employed here. Only the thioacetal bridge, which violates the twofold symmetry, was split into two conformations; the rest of the antibiotic was modelled with a single conformation. The methyl group in the bridge could not be located in the electron density and was omitted from the model in all four echinomycins.

Table 4
Echinomycin–DNA hydrogen-bonding distances in the crystal.

Donor	Acceptor	Distance (Å)
Ala12 N	G107 N3	2.96
G107 N2	Ala12 O	3.00
Ala17 N	G3 N3	2.84
G3 N2	Ala17 O	3.14
Ala112 N	G7 N3	2.89
G7 N2	Ala112 O	3.05
Ala117 N	G103 N3	2.93
G103 N2	Ala117 O	3.26
Ala212 N	G307 N3	3.04
G307 N2	Ala212 O	3.26
Ala217 N	G203 N3	3.05
G203 N2	Ala217 O	3.13
Ala312 N	G303 N3	3.06
G303 N2	Ala312 O	3.12
Ala317 N	G207 N3	2.95
G207 N2	Ala317 O	3.10

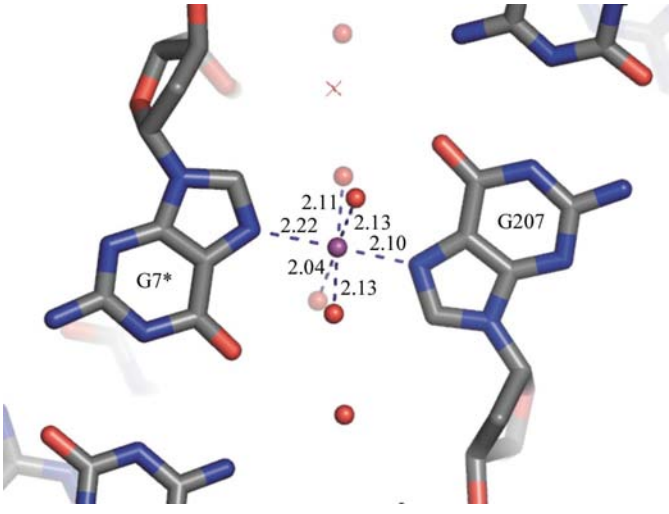

Figure 2
The metal site has a nearly perfect octahedral geometry. It links two different DNA duplexes laterally (an asterisk indicates a symmetry equivalent).

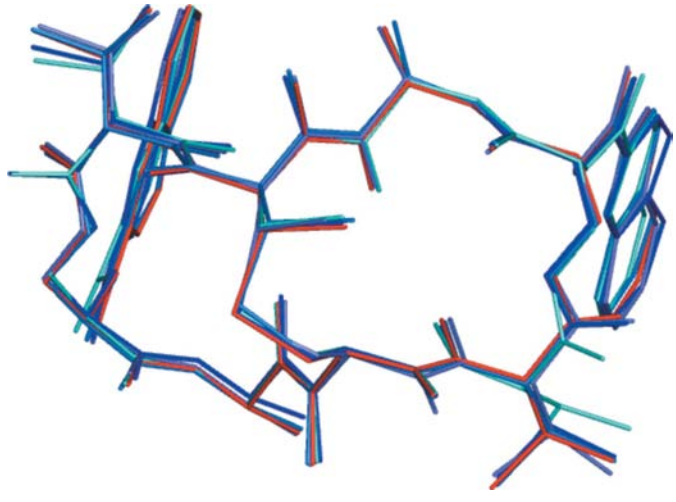

Figure 3
Superposition of all four independent echinomycins (in different blue tones) on that found in 1xvn. Only the main conformations were considered.

The binding of echinomiycin to the DNAs is not significantly affected by the presence of Hoogsteen or Watson–Crick base pairs. All four echinomycins in the crystal bind to the DNA in the same way and form the same four hydrogen bonds between the oxygen and the nitrogen of the alanines and N2 and N3 of both guanines inside the intercalation sites. The hydrogen-bond distances (Table 4) are similar for all four echinomycins and also deviate little from those found in PDB entries 1pfe, 1xvk, 1xvr and 1xvn (Cuesta-Seijo & Sheldrick, 2005).

3.4. Base pairing and DNA structure

All eight base pairs within the bisintercalation sites are in the Watson–Crick configuration, whereas only five of the eight external base pairs are in the Hoogsteen configuration. In this crystal form, adenines 5, 101 and 105 are all in the *anti* conformation and undergo standard Watson–Crick base pairing with thymines 104, 8 and 4, respectively (Fig. 4). These three base pairs are in the same DNA duplex, which has only one Hoogsteen base pair. The four corresponding base pairs in the other DNA duplex in the asymmetric unit are in the Hoogsteen configuration, as they were in the hexagonal metal-free crystal form 1xvn (Cuesta-Seijo & Sheldrick, 2005). Crystals of the latter form can grow in the same drops as the tetragonal crystals reported here. This reflects the intrinsic flexibility of the structure, as previously suggested by NMR data (Gilbert & Feigon, 1991).

The *B* values for the atoms of the base pairs are in the same range in both duplexes irrespective of whether they are in the Hoogsteen or the Watson–Crick configuration. Furthermore, the terminal base pairs T8–A101 and T208–A301 are involved in crystal-packing contacts, but base pairs T4–A105 and A5–T104 in the Watson–Crick configuration and their Hoogsteen equivalents in the other duplex T204–A305 and A205–T304 are not involved in such contacts. The hydrogen-bond distances for the base pairing are listed in Table 5. The abnormally short values in the range of 2.5 Å correspond to

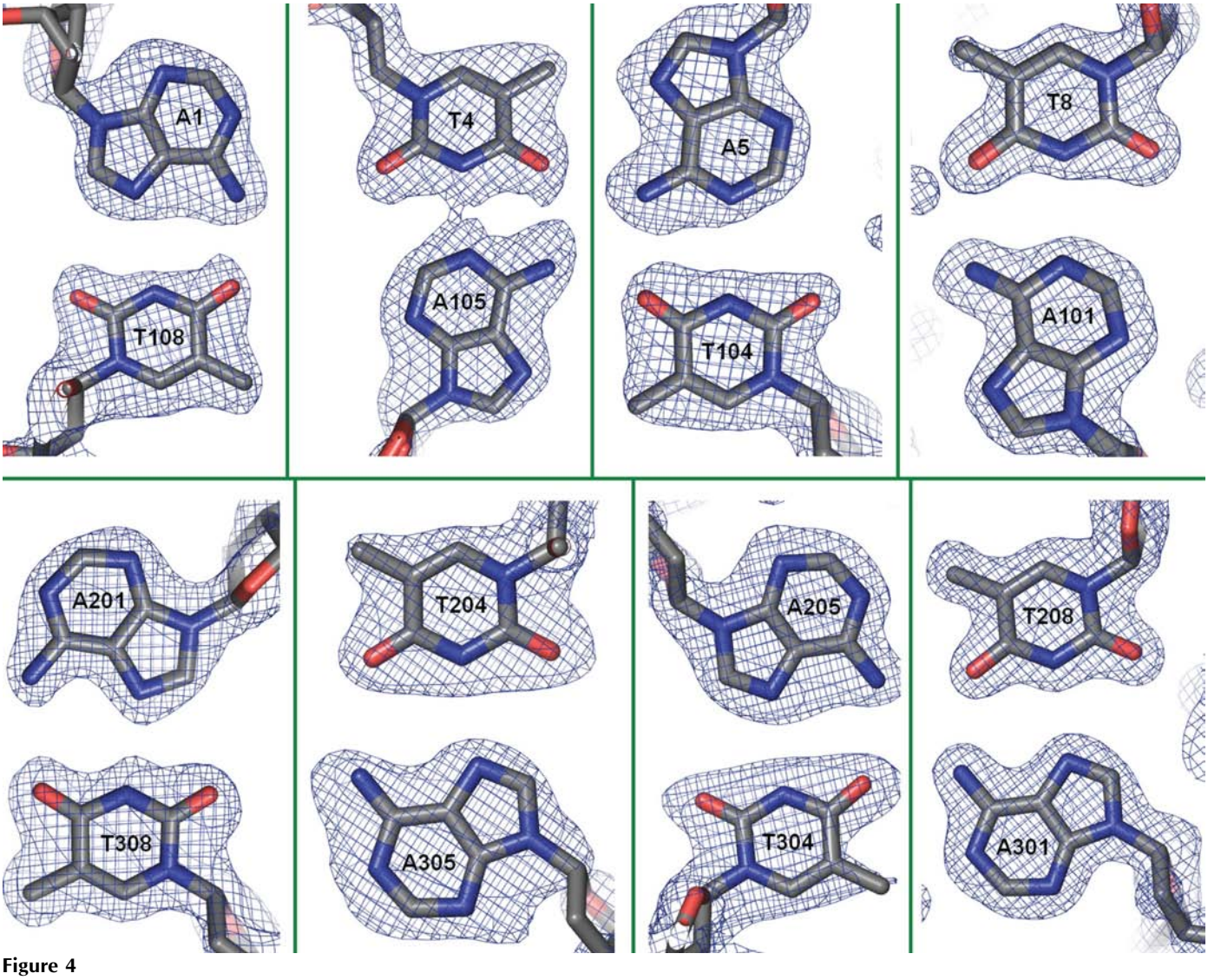

Figure 4
$2F_o - F_c$ electron density contoured at the 1.5σ level for all eight base pairs external to the intercation sites. T4–A105, A5–T104 and T8–A101 (the three right-hand pairs in the top row) are clearly Watson–Crick; the remaining five are Hoogsteen.

the most mobile part of the structure, with average B values of the order of 50 Å^2 for residues A305, C306 and G307. The geometry of these regions should be interpreted with caution, but there was no significant residual density in the difference electron-density maps and it was not necessary to model double conformations for any of the bases.

The overall conformation of the DNA duplexes in this crystal is compared in Fig. 5 with that in 1xvn; superpositions were performed using the *XFIT* program (McRee, 1999). For the second duplex, comprising bases A201–T308, the r.m.s.d. relative to 1xvn is 1.39 Å for the main conformations. For the first duplex the r.m.s.d. relative to 1xvn is 2.15 Å, higher as expected owing to the extra Watson–Crick base pairs. Despite this, all three duplexes exhibit roughly the same conformation, in particular in the direction of the helix axis. The differences are larger in directions perpendicular to the helix axis, where 1xvn showed some degree of disorder. Hoogsteen and Watson–Crick base pairs can be integrated in the structure without very large displacements of the bases, but a widening of the minor groove is apparent for the Watson–Crick configuration relative to the Hoogsteen conformation, with the sugars and phosphate of the backbones further apart from those of the complementary chain in the Watson–Crick cases. Bases G7 and G207, despite coordinating the cation, do not have significantly distorted conformations.

The buckling of the bases internal to the bisintercalation sites is in the range 20–25° (measured with the program 3*DNA*; Lu & Olson, 2003), as was the case for 1xvn, 1pfe and 1xvk. This is necessary to accommodate the quinoxaline bases, which are roughly 10 Å apart and not perfectly parallel to each other. Seven of the eight AT base pairs, all external to the bisintercalation sites, have buckling angles close to 0°, the exception being T8–A101 with a buckle of 14.9° with the bases opening away from the quinoxaline base. Such a pronounced buckle has not been observed for the corresponding base pairs in other crystal structures of complexes between DNA and quinoxaline antibiotics. This base pair is also the only example in these structures of a terminal base pair that is not involved in base stacking on both sides of the bases. One side of the base pair is stacked on the corresponding quinoxaline, but on the other side the shortest contacts involve an ester linkage of another echinomycin and a deoxyribose of a different DNA molecule. As with the other base pairs, it makes close contacts with the quinoxaline, the shortest being 3.0 Å. As was the case for 1xvn, the extent of π-overlap of the quinoxalines with the bases within the bisintercalation sites is relatively small, but is greater with the external bases. For both the Watson–Crick and the Hoogsteen flanking base pairs, the purines lie approximately over the chromophore 2-carbonyl groups.

Complexing of echinomycin introduces unwinding in the DNA. Measuring this unwinding angle is not a trivial operation, since the presence of the Hoogsteen base pairs makes it difficult to define a helix axis. An approximation is to measure the virtual torsion angle defined by the four C1′ C atoms in two different base pairs. Measuring twist angles in this way and subtracting them from a reference value of 36° for B-DNA (Olson *et al.*, 2001) gives an unwinding angle of 57.3°

Table 5
Hydrogen-bonding distances for the base pairing.

WC stands for Watson–Crick and HG for Hoogsteen base pairing.

Atoms	Distance (Å)	Type	Atoms	Distance (Å)	Type
A1 N6···T108 O4	2.76	HG	A201 N6···T308 O4	3.15	HG
A1 N7···T108 N3	3.06		A201 N7···T308 N3	2.85	
C2 O2···G107 N2	3.15	WC	C202 O2···G307 N2	2.79	WC
C2 N3···G107 N1	3.03		C202 N3···G307 N1	2.84	
C2 N4···G107 O6	3.00		C202 N4···G307 O6	2.51	
G3 N1···C106 N3	2.79	WC	G203 N1···C306 N3	2.80	WC
G3 N2···C106 O2	2.88		G203 N2···C306 O2	2.88	
G3 O6···C106 N4	2.67		G203 O6···C306 N4	2.49	
T4 N3···A105 N1	2.69	WC	T204 N3···A305 N7	2.83	HG
T4 O4···A105 N6	3.03		T204 O4···A305 N6	3.06	
A5 N1···T104 N3	2.89	WC	A205 N6···T304 O4	2.94	HG
A5 N6···T104 O4	2.86		A205 N7···T304 N3	2.90	
C6 O2···G103 N2	2.80	WC	C206 O2···G303 N2	2.89	WC
C6 N3···G103 N1	2.85		C206 N3···G303 N1	2.86	
C6 N4···G103 O6	2.72		C206 N4···G303 O6	2.77	
G7 N1···C102 N3	2.99	WC	G207 N1···C302 N3	2.95	WC
G7 N2···C102 O2	2.93		G207 N2···C302 O2	2.98	
G7 O6···C102 N4	2.96		G207 O6···C302 N4	2.88	
T8 N3···A101 N1	2.90	WC	T208 N3···A301 N7	2.89	HG
T8 O4···A101 N6	2.86		T208 O4···A301 N6	2.94	

between base pairs A5–T104 and T8–A101, which is consistent with the 55.3° obtained with *3DNA* (Lu & Olson, 2003) for this fully Watson–Crick region. The virtual torsion-angle method gives an unwinding angle of 50.3° between base pairs A1–T108 and T4–A105, containing one Hoogsteen base pair, 61.6° for base pairs A201–T308 and T204–A305 and 65.2° between base pairs A205–T304 and T208–T301, which are all Hoogsteen. Thus, the presence of the Watson–Crick base pairs

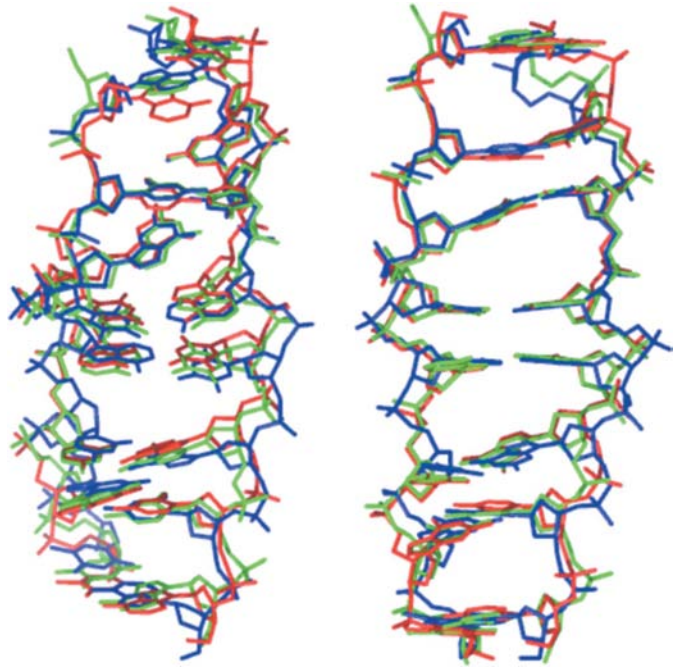

Figure 5
Superposition of the two DNA duplexes of this crystal on those of 1xvn. The duplex comprising residues 1–108, which has Watson–Crick base pairs flanking the bisintercalation site, is shown in blue. The second duplex is in green and that of the hexagonal form (1xvn) is in red. The orientation is similar in both views, with adenine A1 at the top left.

seems to reduce the unwinding induced in the DNA by binding echinomycin.

3.5. The metal site

Both the fluorescence scans and the anomalous maps indicate that the unexpected metal site is occupied by nickel and zinc only. This does not necessarily mean that the binding site is only capable of binding nickel and zinc or that the occupancies are indicative of the relative affinities for these cations. They were not knowingly introduced in the crystallization trials and their concentrations in the drop remain unknown. Further crystallization tests with transition-metal cations as additives indicated that Cu^{2+} can also promote the growth of crystals of this crystal form, at least at low concentrations (it inhibits growth when present at higher concentration), suggesting that the metal-binding site is able to bind a range of cations based on availability.

4. Conclusions

A new crystal form was obtained for the complex between $(ACGTACGT)_2$ and echinomycin. The structure was phased serendipitously by the SAD method based on a single unexpected anomalous scatterer that could subsequently be identified as a mixture of nickel and zinc by fluorescence scans and by measurements of the anomalous scattering at different wavelengths. This cation is coordinated octahedrally by two guanines from two different duplexes (*trans* to one another) and four water molecules. The fact that a single unexpected cation was adequate to solve the phase problem, although the wavelength had not been chosen to maximize the anomalous signal and the data had not been collected with the use of the anomalous differences in mind (for which a higher redundancy would normally have been employed), suggests that the intentional introduction of such cations could have considerable potential for the solution of DNA-containing structures (and possibly also for the production of new crystal forms).

The structure was refined to a resolution of 1.6 Å and resembles previously reported crystal structures of DNA–echinomycin complexes except that for three of the base pairs flanking the echinomycin bisintercalation sites the purines are in the *anti* conformation and the base pairs are standard Watson–Crick. This is the first observation in a crystal of Watson–Crick base pairs external and adjacent to the bisintercalation sites of quinoxaline antibiotics. The Hoogsteen configuration was found for the corresponding base pairs of the crystallographically independent duplex, indicating that the two configurations are almost equal in energy, in agreement with NMR data (Gilbert & Feigon, 1991). The structure accommodates either Watson–Crick or Hoogsteen base pairs in these positions without significant distortion of the geometry beyond that introduced by the echinomycin binding itself and the *syn* or *anti* glycosidic bonds.

We should particularly like to thank Michael J. Waring and Ulf Diederichsen for arousing our interest in this subject and for many discussions. We are grateful to the Fonds der Chemischen Industrie, the Deutsche Forschungsgemeinschaft (SFB416) and to the European Community (Access to Research Infrastructure Action of Improving Human Potential Programme to the EMBL Hamburg Outstation, contract No. HPRI-1999-CT-000017) for support and to EMBL/DESY, Hamburg and BESSY, Berlin for generous allocations of beamtime.

References

Brünger, A. T. (1992). *Nature (London)*, **355**, 472–475.
Cromer, D. T. & Liberman, D. (1970). *J. Chem. Phys.* **53**, 1891–1898.
Cuesta-Seijo, J. A. & Sheldrick, G. M. (2005). *Acta Cryst.* D**61**, 442–448.
Gallego, J., Luque, F. J., Orozco, M., Burgos, C., Alvarez-Builla, J., Rodrigo, M. M. & Gago, F. (1994). *J. Med. Chem.* **37**, 1602–1609.
Gallego, J., Luque, F. J., Orozco, M. & Gago, F. (1994). *J. Biomol. Struct. Dyn.* **12**, 111–129.
Gao, X. & Patel, D. J. (1988). *Biochemistry*, **27**, 1744–1751.
Gilbert, D. E. & Feigon, J. (1991). *Biochemistry*, **20**, 2483–2494.
Gilbert, D. E. & Feigon, J. (1992). *Nucleic Acids Res.* **20**, 2411–2420.
Jeppesen, C. & Nielsen, P. E. (1988). *FEBS Lett.* **231**, 172–176.
Kabsch, W. (1993). *J. Appl. Cryst.* **26**, 795–800.
Leslie, K. D. & Fox, K. R. (2002). *Biochemistry*, **41**, 3484–3497.
Lu, X.-J. & Olson, W. K. (2003). *Nucleic Acids Res.* **31**, 5108–5121.
McLean, M. J., Seela, F. & Waring, M. J. (1989). *Proc. Natl Acad. Sci. USA*, **86**, 9687–9691.
McRee, D. (1999). *J. Struct. Biol.* **125**, 156–165.
May, L. G., Madine, M. A. & Waring, M. J. (2004). *Nucleic Acids Res.* **32**, 65–72.
Olson, W. K., Bansal, M., Burley, S. K., Dickerson, R. E., Gerstein, M., Harvey, S. C., Heinemann, U., Lu, X. L., Neidle, S., Shakked, Z., Sklenar, H., Suzuki, M., Tung, C. S., Westhof, E., Wolberger, C. & Berman, H. M. (2001). *J. Mol. Biol.* **313**, 229–237.
Otwinowski, Z. & Minor, W. (1997). *Methods Enzymol.* **276**, 307–326.
Pape, T. & Schneider, T. R. (2004). *J. Appl. Cryst.* **37**, 843–844.
Park, J. Y., Park, S. J., Shim, K. Y., Lee, K. J., Kim, Y.-B., Kim, Y. H. & Kim, S. K. (2004). *Pharm. Res.* **50**, 201–207.
Portugal, J., Fox, K. R., McLean, M. J., Richenberg, J. L. & Waring, M. J. (1988). *Nucleic Acids Res.* **16**, 3655–3670.
Quigley, G. J., Ughetto, G., van der Marel, G. A., van Boom, J. H., Wang, A. H.-J. & Rich, A. (1986). *Science*, **232**, 1255–1258.
Sato, K., Shiratori, O. & Katagiri, K. J. (1967). *J. Antibiot.* **20**, 270–276.
Sayers, E. W. & Waring, M. J. (1993). *Biochemistry*, **32**, 9094–9107.
Schneider, T. R. & Sheldrick, G. M. (2002). *Acta Cryst.* D**58**, 1772–1779.
Sheldrick, G. M. (2002). *Z. Kristallogr.* **217**, 644–650.
Sheldrick, G. M., Hauptman, H. A., Weeks, C. M., Miller, M. & Usón, I. (2001). *International Tables for Macromolecular Crystallography*, Vol. *F*, edited by M. G. Rossmann & E. Arnold, pp. 333–345. Dordrecht: Kluwer Academic Publishers.
Sheldrick, G. M. & Schneider, T. R. (1997). *Methods Enzymol.* **277**, 319–343.
Tseng, T. D., Ge, H., Wang, X., Edwardson, J. M., Waring, M. J., Fitzgerald, W. J. & Henderson, R. M. (2005). *J. Mol. Biol.* **245**, 745–758.
Ughetto, G., Wang, A. H.-J., Quigley, G. J., van der Marel, G. A., van Boom, J. H. & Rich, A. (1985). *Nucleic Acids Res.* **13**, 2305–2323.
Wakelin, L. P. G. & Waring, M. J. (1976). *Biochem. J.* **157**, 721–740.
Ward, D. C., Reich, E. & Goldberg, I. H. (1965). *Science*, **149**, 1259–1263.
Wang, A. H.-J., Ughetto, G., Quigley, G. J., Hakoshima, T., van der Marel, G. A., van Boom, J. H. & Rich, A. (1984). *Science*, **225**, 1115–1121.

Wang, A. H.-J., Ughetto, G., Quigley & Rich, A. (1986). *J. Biomol. Struct. Dyn.* **4**, 319–342.
Waring, M. J. (1981). *Annu. Rev. Biochem.* **50**, 159–192.
Waring, M. J. (1993). *Molecular Aspects of Anticancer Drug–DNA Interactions*, edited by S. Neidle & M. J. Waring, Vol. 1, pp. 213–242. London: MacMillan.
Waring, M. J. & Wakelin, L. P. G. (1974). *Nature (London)*, **252**, 653–657.